Reducing microtubule detyrosination improves heart function in HCM mice and human iPSC-engineered heart tissues

Niels Pietsch[1,2], Christina Y. Chen[3,4], Svenja Kupsch[5,6], Lucas Bacmeister[5,7], Birgit Geertz[1], Marisol Herrera-Rivero[8,9], Hanna Voß[10], Elisabeth Krämer[1], Ingke Braren[11], Dirk Westermann[2,5,7], Hartmut Schlüter[10], Giulia Mearini[1,2,12], Saskia Schlossarek[1,2], Jolanda van der Velden[12], Matthew Caporizzo[3,13], Diana Lindner[2,5,7], Benjamin L. Prosser[3], Lucie Carrier[1,2,*]

[1]Department of Experimental Pharmacology and Toxicology, University Medical Center Hamburg-Eppendorf, Hamburg, Germany;

[2]DZHK (German Centre for Cardiovascular Research), partner site Hamburg/Kiel/Lübeck, Hamburg, Germany;

[3]Department of Physiology, Pennsylvania Muscle Institute, University of Pennsylvania Perelman School of Medicine, Philadelphia, PA 19104, USA;

[4]Gene Therapy Program, Department of Medicine, Perelman School of Medicine, University of Pennsylvania, Philadelphia, PA, USA (current affiliation);

[5]Department of Cardiology, University Heart and Vascular Center, University Medical Center Hamburg-Eppendorf, Hamburg, Germany;

[6]Institute of Experimental Cardiovascular Research, University Medical Center Hamburg-Eppendorf, Hamburg, Germany (current affiliation);

[7]Department of Cardiology and Angiology, University Heart Center Freiburg-Bad Krozingen, Faculty of Medicine, University of Freiburg, Freiburg, Germany (current affiliation);

[8]Department of Genetic Epidemiology, Institute of Human Genetics, University of Münster, Münster, Germany;

[9]Department of Psychiatry, University of Münster, Münster, Germany (current affiliation);

[10]Section Mass Spectrometric Proteomics, University Medical Center Hamburg-Eppendorf, Hamburg, Germany (current affiliation);

[11]Vector facility, Department of Experimental Pharmacology and Toxicology, University Medical Center Eppendorf, Hamburg, Germany;

[12]DiNAQOR AG, 8952 Schlieren, Switzerland (current affiliation);

[13]Amsterdam UMC, Vrije Universiteit Amsterdam, Department of Physiology, Amsterdam Cardiovascular Sciences, Amsterdam, The Netherlands.

[13]Department of Molecular Physiology and biophysics, University of Vermont Larner College of Medicine, Burlington, VM, USA (current affiliation);

Short title: Reducing tubulin detyrosination in hearts

*Corresponding author: Lucie Carrier, Department of Experimental Pharmacology and Toxicology, University Medical Center Hamburg-Eppendorf, Hamburg, Germany, Martinistrasse 52, 20246 Hamburg, Germany, Phone: +49-40-7410-57208; Email: l.carrier@uke.de

Word count: 8,069

Abstract

Rationale: Hypertrophic cardiomyopathy (HCM) is the most common cardiac genetic disorder caused by sarcomeric gene variants and associated with left ventricular (LV) hypertrophy and diastolic dysfunction. The role of the microtubule network has recently gained interest with the findings that α-tubulin detyrosination (dTyr-tub) is markedly elevated in heart failure. Reduction of dTyr-tub by inhibition of the detyrosinase (VASH/SVBP complex) or activation of the tyrosinase (tubulin tyrosine ligase, TTL) markedly improved contractility and reduced stiffness in human failing cardiomyocytes, and thus poses a new perspective for HCM treatment.
Objective: In this study, we tested the impact of targeting dTyr-tub in a mouse model of HCM, the *Mybpc3*-targeted knock-in (KI) mice, and in human induced pluripotent stem cell (hiPSC)-derived cardiomyocytes and engineered heart tissues (EHTs) deficient in SVBP or TTL.
Methods and Results: TTL gene transfer was tested in wild-type (WT) mice and rats and in adult KI mice. We show that i) TTL dose-dependently reduced dTyr-tub and improved contractility without affecting cytosolic calcium transients in WT cardiomyocytes; ii) TTL partially improved LV function and diastolic filling, reduced stiffness and normalized cardiac output and stroke volume in KI mice; iii) TTL induced a marked transcription and translation of several tubulins in KI mice; iv) TTL modulated mRNA or protein levels of components of mitochondria, Z-disc, ribosome, intercalated disc, lysosome and cytoskeleton in KI mice; v) SVBP-KO and TTL-KO EHTs exhibited low and high dTyr-tub levels, higher and lower force of contraction and enhanced and prolonged relaxation than in WT EHTs, respectively. RNA-seq and mass spectrometry analysis revealed distinct enrichment of cardiomyocyte components and pathways in SVBP-KO vs. TTL-KO EHTs.
Conclusion: This study provides evidence that reducing dTyr-tub improves function in HCM mouse hearts and human EHTs and holds promise for targeting the non-sarcomeric cytoskeleton in heart disease.

Keywords:

heart function; hypertrophic cardiomyopathy; engineered heart tissue; hiPSC; tubulin detyrosination

Introduction

Hypertrophic cardiomyopathy (HCM) is the most common inherited cardiac disease caused by mutations in several sarcomeric genes. *MYBPC3*, encoding cardiac myosin-binding protein C is the most frequently mutated gene.[1] HCM is associated with left ventricular (LV) hypertrophy, diastolic dysfunction and increased interstitial fibrosis. Treatment of severe HCM with outflow tract obstruction is limited to surgical removal of septal tissue or catheter ablation.

The role of the microtubule network during progression of cardiac diseases has gained interest in recent years with the findings that microtubule detyrosination and associated cardiomyocyte stiffness is elevated in HCM and heart failure[2, 3] (for reviews,[4-7]). The cycle of α-tubulin detyrosination/re-tyrosination consists in the catalytic removal and re-incorporation of the last C-terminal tyrosine of α-tubulin. We have previously reported higher levels of detyrosinated tubulin (dTyr-tub) in human and mouse models of HCM.[2, 8] The tubulin tyrosine ligase (TTL) catalyses the tyrosination, and the tubulin carboxypeptidase complex, composed of vasohibin (VASH1 or VASH2) and its chaperone, the small vasohibin-binding protein (SVBP), catalyses the removal of the C-terminal tyrosine. VASH1 is the major isoform in human heart.[9] Recently, it was shown that reduction of dTyr-tub by *TTL* overexpression or *VASH1* knockdown markedly improved contractility and reduced stiffness in human failing cardiomyocytes[8, 9] and thus poses a possible new perspective for the treatment of HCM.

In this study, we evaluated the impact of adeno-associated virus serotype 9 (AAV9)-mediated *TTL* gene transfer in neonatal wild-type (WT) rodents and in 3-week-old homozygous *Mybpc3*-targeted knock-in (KI) mice that present with eccentric LV hypertrophy and both systolic and diastolic dysfunction.[10, 11] Using a combination of approaches, we show that TTL lowered dTyr-tub, improved contractility without affecting calcium transients in WT rat cardiomyocytes, and partially improved LV function, diastolic filling, compliance, stroke volume and cardiac output in KI mice. We further provide evidence that TTL did not significantly affect the fetal gene program and LV hypertrophy but modulates the TTL modulated mRNA or protein levels of components of mitochondria, Z-disc, ribosome, intercalated disc, lysosome and cytoskeleton in KI mice. These data were supported by the generation of SVBP- and TTL-deficient human induced pluripotent stem cell (hiPSC)-derived cardiomyocytes and engineered heart tissues (EHTs) from a control hiPSC line with CRISPR/Cas9 genetic tools.

Methods

Animals

The investigation conforms to the guidelines for the care and use of laboratory animals published by the NIH (Publication No. 85-23, revised 1985). For studies in WT C57BL/6J mice and Sprague-Dawley rats, animal care and use procedures were approved and performed in accordance with the standards set forth by the University of Pennsylvania Institutional Animal Care and Use Committee and the Guide for the Care and Use of Laboratory Animals published by the US National Institutes of Health. KI mice were generated previously,[10] and both KI and WT mice were maintained on a Black Swiss background. The experimental procedures performed in KI and WT mice were in accordance with the German Law for the Protection of Animals and accepted by the Ministry of Science and Public Health of the City State of Hamburg, Germany (Nr. 074-19).

Isolation of adult mouse and rat ventricular myocytes and functional assessment

Primary ventricular cardiomyocytes were isolated as previously described.[12] Briefly, the heart was removed from 6-week-old mouse or rat anesthetized under isoflurane and retrograde-perfused on a Langendorff apparatus with a collagenase solution. The digested heart was then minced and triturated using a glass pipette. The resulting supernatant was separated and centrifuged at 300 revolution per minute (rpm) to isolate cardiomyocytes which were then

resuspended in cardiomyocyte media for functional assessment. Elastic modulus was measured using nanoindentation (Piuma Chiaro, Optics11, The Netherlands) as previously described.[13] Cardiomyocytes contractility and calcium transients were measured as previously described.[9]

Human iPSC-derived cardiomyocytes and EHT contractility measurements

A control hiPSC line carrying a monoallelic mTag-RFP-T-TUBA1B (clone AICS-0031-035, Allen Institute for Cell Science, Seattle, WA, USA) was expanded and used to create SVBP-KO and TTL-KO hiPSC lines with CRISPR/Cas9 technology. Two sgRNAs were selected for each locus to create a large deletion (Figure S1A). Cells were nucleofected using the Amaxa 4D nucleofector (Lonza) with pre-annealed ribonucleoprotein complexes of sgRNAs and recombinant Cas9 protein (IDT, 1081058), single cell clones expanded and genotyped for successful homozygous deletions (Figure S1B). Clones with large homozygous deletions for each of the genes of interest underwent quality control in karyotyping (Figure S1C) by nCounter profiling (NanoString, Seattle, US), pluripotency validation by SSEA-3 (stage-specific embryonic antigen 3) staining (BD Biosciences, 560892; Figure S1D) and control for mycoplasma contamination. To ensure specific activity of the CRISPR-Cas9 system, the 10 most likely off-target loci were identified with crispor.tefor.net,[14] and sequenced to assess genome integrity. No alterations were detected, indicating no unspecific activity of the CRISPR-Cas9 complex (data not shown). After expansion of the 3 hiPSC lines, cardiomyocytes were produced according to the monolayer protocol.[15] RT-qPCR was performed with RNA isolated from hiPSC-CMs to ensure mRNA deficiency of the respective gene (Figure S1E,F).

EHTs were casted from 2-6 independent batches of cardiomyocyte differentiation of the 3 hiPSC lines on standard silicone posts (0.28 mN/mm) or on stiffer silicone that induced afterload enhancement (0.8 mN/mm). Auxotonic contractions were measured until day 60 as previously described.[16-18]

Plasmid constructs and AAV9 particle production

The TTL-IRES-dsRed insert was cloned into an expression construct flanked by AAV2 inverted terminal repeats containing a human cardiac troponin T (cTnT) promotor, a chimeric intron, a post-transcriptional regulatory element (WPRE) and a rabbit beta-globin poly A sequence (PENN.AAV.cTNT.TTL.IRES.dsRed; Figure S2A). AAV9 pseudotyped vector was generated by triple transfection of HEK293 cells and iodixanol purification (Penn Vector Core, University of Pennsylvania) as previously described.[19] Genome copy titer was determined using a droplet digital PCR-based method.[20]

The pGG2-*TNNT2*-*HA*-*TTL* and the pAAV-*TNNT2*-Empty plasmids were generated from the pGG2-*TNNT2*-Mut1 plasmid (VC206) by InFusion Cloning (Takara Clontech). In brief, the full-length HA-TTL was amplified from the HA-TTL-IRES-dsRed plasmid using PrimeStar GLX Polymerase (Takara Clontech) and ligated into the NheI and Bam*H*I restriction sites of VC206. The Empty plasmid was generated by amplification of the *TNNT2* promoter region from VC206 plasmid and inserted into MluI and HindIII restriction sites of pAAV-GFP (Cellbiolabs). After ligation, ampicillin-resistant clones were tested by enzymatic digestion for presence of the insert and one positive clone of each pGG2-*TNNT2*-*HA*-*TTL* and pAAV-*TNNT2*-Empty was sequenced. AAV9 pseudotyped vectors were generated by triple transfection of HEK293 cells with pGG2-*TNNT2*-*HA*-*TTL* or pAAV-*TNNT2*-Empty, pE8/9 (kindly provided by Julie Johnston, Penn Vector Core, University of Pennsylvania, PA, USA) and pHelper encoding adenoviral helper functions (Cellbiolabs). Generation of recombinant AAV9 particles was carried out as described previously.[21, 22]

In vivo AAV9 administration

Neonatal WT C57BL/6 mice received (sc) AAV9-TTL-dsRed at a dose of 1.75E11 or 9E11 vg/g at postnatal day 2 (P2). Neonatal Sprague Dawley rats received AAV98-TTL-dsRed at a dose of 4.4E11 vg/g at P4 (pericardial injection). Three-week-old WT and KI mice received

AAV9 encoding either an empty cassette (AAV9-Empty) or HA-tagged TTL (AAV9-TTL) at a dose of 2.25E11 vg/g via systemic administration into the tail vein using a 30-G needle.[21-23]

Echocardiographic analysis in mice
Transthoracic echocardiography was performed using the Vevo 3100 System (VisualSonics, Toronto, Canada) as described previously.[21-23]

Hemodynamic measurements in mice
Hemodynamic measurements were performed using a PV loop system (ADV500, Transonic) in closed-chest approach.[24, 25] Mice were anesthetized using urethane (0.8-1.2 g/kg body weight) and buprenorphine analgesia (0.1 mg/kg body weight), intubated and artificially ventilated. A pressure-conductance catheter (1.2F, Transonic) was inserted in the right carotid artery and carefully pushed forward into the LV. Catheter's position inside the ventricle was optimized until rectangular-shaped loops were obtained. PV loops were conducted under short-time apnoea. During the PV loop measurements, inferior vena cava (IVC) was occluded by gentle compression. To estimate the volume, a bolus of hypertonic saline (10%) was injected into the left jugular vein.[26] Data were acquired using iox2 (Emka Technologies). Heart rate, maximum rate of LV pressure development in systole (dP/d_{tmax}), maximal rate of LV pressure development in diastole (dP/dt_{min}), LV end-diastolic pressure (LVEDP) and volume (LVEDV), and LV end-systolic pressure (LVESP) and volume (LVESV) were measured. Subsequent analyses of PV loops were performed in LabChart 7.3Pro (AD Instruments). For baseline analysis, 5-10 consecutive loops during end-expiratory ventilation pause were selected to calculate preload-dependent parameters. Preload-independent parameters were analysed by selecting loops during IVC occlusion.[26] Only mice that underwent appropriate levels of anaesthesia, did not experience excessive bleeding during the procedure, and had technically sufficient measurements were included in the analysis

Protein extraction and Western blot analysis
For experiments performed in neonatal mice, Western blot of whole heart protein extraction was performed to quantified TTL (1:500; Proteintech, 13618-1-AP), α-tubulin (1:1000; clone DM1A, Cell Signaling, 3873), dTyr-tub (1:1000; Abcam, ab48389) and dsRed protein levels as previously described.[9] For the other experiments, Western blots were performed as described previously.[10, 21, 22] In brief, crude protein fractions were extracted from mouse hearts or 30 day-old 2D hiPSC-derived cardiomyocytes, separated on 12% SDS-polyacrylamide (29:1) mini-gels (Bio-Rad) and electrotransferred on PVDF or nitrocellulose membranes as previously described.[10] Primary antibodies were directed against the HA epitope (1:2000; Sigma, H3663), dTyr-tub and α-tubulin (1:2000 and 1:5000; both kindly provided by Marie-Jo Moutin, Grenoble, France), or GAPDH (1:2,000; HyTest). Secondary antibodies were peroxidase-conjugated anti-mouse (1:20,000, Dianova) or anti-rabbit (1:6,000, Sigma). Proteins were visualized with Clarity Western ECL substrate (Bio-Rad) and signals were detected with the ChemiGenius² Bio Imaging System.

Titin isoform analysis on crude mouse protein fractions
Titin isoforms were separated on a 1% w/v agarose gel and stained with SYPRO Ruby protein gel stain (Invitrogen, ThermoFisher Scientific) as previously described.[27] All samples were measured in triplicate and the average of triplicate measurements per sample was shown.

Immunofluorescence analysis of hiPSC-cardiomyocytes
2D-culture of cardiomyocytes from the 3 hiPSC lines were seeded onto black, geltrex-coated 96-well plates (ThermoFisher Scientific, 165305) with 90.000 cells/cm^2 and cultured in low glucose DMEM-based medium for 30 days until cells were washed with PBS and fixed with ROTI®Histofix (Carl Roth, P087.1) for 10 min at 4 °C. For immunofluorescence imaging, cells were incubated with blocking buffer (PBS containing 3 % milk and 0.1 % Triton X-100) and primary antibodies against ACTN2 (1:800, Sigma, A7811) and dTyr-tub (1:1000, kindly provided by Marie-Jo Moutin, Grenoble, France) overnight. Cells were washed with PBS and

incubated with secondary antibodies AF-488 rabbit and AF-647 mouse (1:800, ThermoFisher Scientific) in blocking buffer for 90 min at RT. Hoechst 33342 (Invitrogen, H3570) was added 1:2500 for 20 min to stain DNA. Image acquisition was performed with a Zeiss LSM 800 confocal microscope.

RNA-sequencing

For RNA-sequencing (RNA-seq), total RNA was isolated from LV samples of female WT-Empty, KI-Empty, and KI-TTL mice (N=3 per group) using the Direct-zol RNA Microprep Kit (Zymo Research) followed by a DNase digestion step. Enrichment of mRNAs with the NEBNext Poly(A) mRNA Magnetic Isolation Module was followed by library preparation using the NEBNext Ultra II RNA Directional Library Prep Kit for Illumina (New England BioLabs). Single read sequencing took place on a NextSeq 2000 System (Illumina), using the corresponding NextSeq 2000 P3 Reagents (50 cycles), with a read length of 72 base pairs. The integrity of the RNA and quality of the library were assessed using a TapeStation 4200 (Agilent).

The sequencing data was automatically demultiplexed using the Illumina BCL Convert Software v3.8.2. FastQ files underwent pre-trimming and post-alignment quality control rounds using FastQC v0.11.7 (https://www.bioinformatics.babraham.ac.uk/projects/fastqc/). Removal of Illumina adapters and low-quality sequences was performed with Trimmomatic v0.38.[28] Reads of length <15 bases, as well as leading and/or trailing bases with quality <3 or no base call, and bases with average quality <15 in a 4-base sliding window were removed. Alignment was performed with HISAT2 v2.1,[29] using the mouse genome assembly mm10 (Mus musculus, GRCm38). Mapped reads (primary alignments) were sorted by read name using SAMtools v1.8,[30] and read counts were calculated with HTSeq v0.11.2.[31]

Differential expression was assessed using DESeq2[32] for all possible comparisons. Raw read counts were filtered to remove genes with less than 10 counts prior to analysis. Here, statistical significance of coefficients was tested using a negative binomial generalized linear model with the Wald test and p-values were adjusted for multiple comparisons following the Benjamini-Hochberg method (Padj). Genes were considered differentially expressed at P or Padj < 0.05 values.

To provide a biological context, each list of differentially expressed genes (DEGs) was subjected to functional enrichment analysis using the web tool g:GOSt from g:Profiler.[33] All gene ontology (GO) and pathways gene set categories available for Mus musculus or Homo sapiens within this tool were retrieved. Gene sets were considered significantly enriched following a hypergeometric test for overrepresentation within annotated genes, corrected for multiple comparisons using the Benjamini-Hochberg method (Padj<0.05).

Mass spectrometry

Mouse LV tissue were lysed in 100 mM triethyl ammonium bicarbonate (TEAB) and 1% w/w sodium deoxycholate (SDC) buffer, boiled at 95 °C for 5 min. Samples were sonicated with a probe sonicator for 6 pulses to destroy DNA/RNA. For proteome analysis 20 µg of protein of each sample was taken and disulfide bonds reduced in the presence of 10 mM dithiothreitol (DTT) at 60 °C for 30 min. Cysteine residues were alkylated in presence of 20 mM iodoacetamide at 37 °C in the dark for 30 min and tryptic digestion (sequencing grade, Promega) was performed at a 100:1 protein to enzyme ration at 37 °C overnight. Digestion was stopped and SDC precipitated by the addition of 1% v/v formic acid (FA). Samples were centrifuged at 16,000 g for 5 min and the supernatant was transferred into a new tube. Samples were dried in a vacuum centrifuge.

Samples were resuspended in 0.1% FA and transferred into a full recovery autosampler vial (Waters). Chromatographic separation was achieved on a nano-UPLC system (Dionex Ultimate 3000 UPLC system, Thermo Fisher Scientific) with a two-buffer system (buffer A: 0.1% FA in water, buffer B: 0.1% FA in ACN). Attached to the UPLC was a reversed phase trapping column (Acclaim PepMap 100 C18 trap; 100 µm x 2 cm, 100 Å pore size, 5 µm particle size, Waters) for desalting; a purification followed by a reversed phase capillary column (nanoEase M/Z peptide BEH130 C18 column; 75 µm x 25 cm, 130 Å pore

size, 1.7-µm particle size, Waters). Peptides were separated using a 60-min gradient with increasing ACN concentration from 2%-30% ACN. The eluting peptides were analyzed on a quadrupole orbitrap ion trap tribrid mass spectrometer (Fusion, Thermo Fisher Scientific) in data dependent acquisition (DDA) mode. For DDA analysis, the fusion was operated at top speed mode analyzing the most intense ions per precursor scan ($2x10^5$ ions, 120,000 Resolution, 120 ms fill time) within 3 s and were analyzed by MS/MS in the ion trap (HCD at 30 normalized collision energy, $1x10^4$ ions, 60-ms fill time) in a range of 400–1300 m/z. A dynamic precursor exclusion of 20 s was used.

NanoString RNA analysis

Total RNA was extracted from powdered whole heart tissue samples using the SV Total RNA isolation kit (Promega, Madison, WI, USA) according to the manufacturer`s instructions. RNA concentration, purity and quality were determined using the NanoDrop® ND-1000 spectrophotometer (Thermo Fisher Scientific). For gene expression analysis, customized NanoString's nCounter® Elements TagSet panels were used. About 50 ng RNA of each sample were hybridized to the target-specific capture and reporter probes at 67 °C overnight (16 h) according to manufacturer's instructions. Samples were cooled down to 4 °C, supplemented with 15 µl H2O, and loaded into the NanoString cartridge. Afterwards the nCounter Gene Expression Assay was started immediately. Raw data were analyzed with the nCounter® Sprint Profiler. Transcript levels were determined with the nSolver™ Data Analysis Software including background subtraction using negative controls and normalization to six housekeeping genes (*Abcf1, Actb, Cltc, Gapdh, Pgk1 and Tubb5*). Data are expressed as Log2 ratio over WT-Empty or KI-Empty.

Statistical analysis

Data were expressed as mean ± SEM. Statistical analyses were performed by one-way or two-way ANOVA followed by Tukey's or Dunnett's post-test, and by unpaired Student's t-test as indicated in figure legends or text, using the commercial software GraphPad Prism8 (GraphPad Software Inc., Boston, US). A value of $P<0.05$ was considered statistically significant.

Results

TTL overexpression leads to a dose-dependent reduction in myocyte stiffness and improved contractility in adult ventricular myocytes

We first evaluated the effect of TTL overexpression for reducing myocardial dTyr-tub level in healthy C57/BL6J mice. For an initial study we tested two different doses of AAV9 (1.75E11 and 9E11 vg/g) encoding TTL-dsRed driven under the *TNNT2* promoter (Figure S2A). Mice were injected at P2 and after 6 weeks of expression myocardial tissue was harvested (Figure 1A). As expected, TTL levels increased in the myocardium in a dose-dependent manner, which was concomitant with decreased dTyr-tub level (Figure 1B). A strong inverse correlation was observed across myocardial samples between increased dsRed and reduced dTyr-tub levels, suggesting that dsRed can be utilized as a useful indicator of dTyr-tub level (Figure 1C).

We next evaluated isolated cardiomyocyte function upon TTL overexpression. We injected a single intermediate dose of AAV9-TTL-dsRed into P4 rats (4.4E11 vg/g; Figure S2A), and isolated single cardiomyocytes 6 weeks later (Figure 1D). Rat myocytes were used for their robustness for functional characterization in our hands.[8, 9] We took advantage of the heterogeneous expression of TTL-dsRed between cardiomyocytes from a given heart to compare myocyte properties to non-expressing controls from the same animal. Myocytes from transduced hearts could be binned into tertiles based on their TTL level (measured by dsRed intensity): 1) those expressing no/low levels of TTL (dsRed intensity within the range of uninjected myocytes), 2) those with moderate TTL expression (10-20x increase in dsRed level

compared to control mean), and 3) those with high TTL overexpression (>20x increase in dsRed level).

Myocytes were assessed for changes in myocyte stiffness, intracellular calcium dynamics and unloaded shortening upon TTL overexpression. Following the functional assessment (blind to expression level), myocytes were binned into TTL expression tertiles. Myocytes expressing TTL showed a dose-dependent reduction in myocyte viscoelasticity as measured via transverse nanoindentation (Figure 1E). Consistent with reduced internal stiffness, myocytes showed a TTL dose-dependent increase in fractional shortening and contractile kinetics (Figure 1F), which appeared to be independent of any changes in intracellular calcium cycling (Figure 1G). This data reflects previous observations obtained in human failing and non-failing cardiomyocytes after acute (48 h) adenoviral-mediated TTL overexpression,[9] and suggests that the rapid reduction in myocyte stiffness and improved contractility (independent of calcium transient alterations as previously shown[8]) persist with chronic TTL overexpression.

TTL therapy partially rescued the cardiac dysfunction in Mybpc3-targeted KI mice

Next, we evaluated whether TTL therapy could rescue the cardiac disease phenotype of the HCM KI mice *in vivo*. KI mice developed LV hypertrophy combined with systolic and diastolic dysfunction.[10, 11] AAV9-Empty or AAV9-TTL vectors were systemically delivered with a dose of 2.25E+11 vg/g in 3-week-old WT and KI mice (Figure S2B,C). Cardiac function was evaluated by serial echocardiography 1, 2, 4, 8, and 12 weeks after treatment (Table S1). After 12 weeks of treatment, ejection fraction (EF), stroke volume (SV), cardiac output (CO), fractional area change (FAC), and aortic ejection time (AET) were lower in KI-Empty than WT-Empty (Figure 2A-E), whereas left ventricular-to-body weight ratio (LVM/BW) was higher (Figure 2F). TTL therapy partially ameliorated EF, SV and CO, but not FAC, AET and LVM/BW in KI mice. Similar data were obtained for the ventricular-to-BW (VW/BW), and the heart-to-BW (HW/BW), VW/tibia length (TL) and HW/TL ratio (data not shown). Overall, most parameters did not change between KI-TTL and KI-Empty groups, but a trend towards better EF, SV and CO from 4 weeks on after treatment was visible (Table S1). When the difference in parameters were calculated between the last and first echocardiography, EF did not significantly differ between the groups (Figure 2G), whereas both SV and CO were significantly higher in KI-TTL than in KI-Empty mice (Figure 2H,I). Among the parameters of diastolic function, isovolumic relaxation time (IRVT) was prolonged in KI-empty mice, but not rescued by TTL treatment (Table S1). When only female mice were considered, the difference between KI-TTL and KI-Empty mice was stronger, and some of the systolic and hypertrophic parameters were markedly ameliorated, such as EF, SV, CO, VW/BW and VW/TL (Figure S3).

At the end of the 12-week treatment, mice were subjected to hemodynamic measurements by LV catheterization (Figure 3). Global function was lower in KI-Empty than WT-Empty and TTL therapy restored SV, CO and stroke work back to WT levels in KI mice (Figure 3A-C, Table S2). Systolic function was not affected, except for the lower EF and a trend to higher LV end-systolic volume (LVESV) and lower PRSW in KI-Empty mice (Figure 3D-H, Table S2). TTL did not impact on the systolic parameters (Figure 3D-H, Table S2). Diastolic function (dP/dt_{min} and Tau) was impaired in KI-Empty mice and not improved after TTL therapy (Figure 3I,L). On the other hand, whereas the LV end-diastolic volume (LVEDV) and minimal rate of volume change (dV/dt_{min}) did not differ between KI- and WT-Empty, they were both higher after TTL therapy (Figure 3J,K), supporting the higher LV end-diastolic diameter (LVEDD) measured by echocardiography, which already increased after 2 weeks of TTL therapy (Table S1). PV loops of a representative mouse of each group at different stages of the occlusion showed higher LV pressure and lower SV in KI-Empty and a marked increase in LVEDV in KI-TTL mouse, resulting in a higher SV (Figure 3M,B,J). This was associated with a reduction in EDPVR (Figure 3N), suggesting reduced stiffness. Taken together, these data provide evidence that TTL therapy improved myocardial compliance and increased diastolic filling to restore CO in KI mice.

TTL therapy partly reduced tubulin detyrosination

Evaluation of cardiac crude protein extracts revealed 37-fold higher TTL level in KI-TTL than in KI-Empty (Figure 4A,B). This was associated with a higher level of total α-tubulin level in KI-TTL (Figure 4A,C) and a trend toward reduced total dTyr-tub level between the groups (Figure 4A,D). However, the dTyr-tub/α-tubulin ratio was 34% and 55% lower in KI-TLL than in WT-Empty and KI-Empty, respectively (Figure 4E). This suggests that TTL increased the abundance of α-tubulins but did not completely suppress dTyr-tub, potentially due to the presence of other detyrosinases in KI-TTL.

TTN isoform switch is not involved in decreased stiffness in KI-TTL

We then evaluated whether the reduction in EDPVR (Figure 3N) is the result of changes in titin isoform composition, leading to less N2B, stiff isoform, and more N2BA, compliant isoform, in KI-TTL. Long-run gel electrophoresis was performed as previously described[27] in LV tissue extracted from the 3 mouse groups. No major difference was detected between the groups in the content of the 3 major isoforms of titin, N2BA, N2B and T2, and therefore in the ratio of N2B/N2BA (Figure 4F,G). This suggests that titin isoform switch does not happen in KI mice and is not involved in the decreased stiffness in KI-TTL.

TTL induced molecular changes in KI mice

To understand the molecular changes induced by TTL gene therapy, RNA-seq and mass spectrometry analyses were performed in female mouse LV tissue extracts (N=3 per group). Differentially expression analysis revealed 1013 dysregulated known mRNAs (263 higher, 750 lower, log2 ratio>0.58 or <-0.58, P<0.05) in KI-Empty than in WT-Empty, and only 104 dysregulated mRNAs (70 higher, 34 lower) in KI-TTL than in KI-Empty (Figure 5A,B). GO pathway analysis of RNA-seq data revealed enrichment (log2 ratio >0.58, P<0.05) in components of the sarcomere, actin cytoskeleton, T-tubule, L-type Ca^{2+} channel, microtubule, with enrichment of cellular and developmental process and transport in KI-Empty vs. WT-Empty (Figure S4A, dataset 1). Since the number of significantly higher and lower mRNAs in KI-TTL vs KI-Empty was low, GO analysis was done on all (log2 ratio >0.58 or <-0.58, P<0.05) and revealed dysregulated metabolic processes and components of mitochondrion, lysosome, nucleus, and late endosome membrane (Figure S4B, dataset 1). Volcano plot of MS analysis revealed much less dysregulated proteins in KI-Empty than in WT (37 higher, 14 lower, log2 ratio >0.58 or <-0.58, P<0.05; Figure 5C) and in KI-TTL than in KI-Empty (11 higher, 9 lower, log2 ratio >0.58 or <-0.58, P<0.05; Figure 5D). MS all pathway analysis in KI-Empty vs. WT-Empty (log2 ratio >0.58 or <-0.58, P<0.05) revealed alterations in components of the sarcomere, succinate-CoA ligase complex, intercalated disk, proteasome complex, and in muscle development and myofibril assembly (Figure S4C, dataset 2). MS all pathway analysis in KI-TTL vs. KI-Empty (log2 ratio >0.58 or <-0.58, P<0.05) revealed changes in components of mitochondria, connective tissue, Z-disc, ribosomal subunits, intercalated disc, and actin cytoskeleton in KI-TTL vs. KI-Empty (Figure S4D, dataset 2).

We then specifically analysed the expression of tubulins and found lower levels of *Tuba1b*, *Tuba4a*, *Tubb5* and *Tubb6* mRNAs in KI-Empty, which were normalized with TTL treatment, and even higher levels of *Tuba4a*, *Tubb2a* and *Tuba8* in KI-TTL than in WT-Empty (Figure 5E). Heatmap revealed marked difference in log2 ratio of tubulin mRNAs between KI-Empty and KI-TTL (Figure 5F). These data were supported by the quantification of selected mRNAs using the nanoString nCounter® Elements technology and customized mouse-specific panels (Table S3). Several genes altered in heart failure were dysregulated in KI-Empty, such as *Myh7*, *Rcan1, Nppb*, *Fhl1*, *Myh6*, *Col1a1*, *Postn*, *Fhl2, Pln* and *Ppp1r1a* (Figure S4E). The levels of mRNAs encoding microtubule-associated proteins, such as *Mapt*, *Clip1*, *Mapre3, KiF5b*, *Map4*, *Dync1h1, Hdac6, Map1lc3a and Actr1a* were higher in KI- than in WT-Empty (Figure S4E). Similarly, the levels of mRNAs encoding proteins of the autophagy-lysosomal pathway such as *Bag3*, *Sqstm1*, *Jak1*, *Lamp1*, *Chmp2b,* and *Epg5* were higher in KI-Empty (Figure S4E), as shown previously in these mice.[34] TTL respectively increased and decreased mRNA levels of several tubulin isoforms and α-tubulin deacetylase *Hdac6* in KI mice (Figure S4F).

Proteomic analysis of tubulins revealed less isoforms than in RNA-seq and an accumulation of all tubulin isoforms in KI- vs WT-Empty and to a higher extent in KI-TTL than in KI-Empty, except for TUBA1A (Figure 5G). Interestingly, tubulin mRNA and protein levels were not correlated in KI-Empty, i.e. lower mRNA levels were associated with higher protein levels than in WT-Empty (Figure 5H) and paralleled what was previously observed in heart failure samples.[35] TTL reversed this correlation and induced the accumulation of most tubulin mRNAs and proteins (Figure 5I). This suggests that KI mice exhibit tubulin protein hyperstability, which could be related to longer lifetimes, increased autoinhibition of tubulin mRNAs, a new concept suggested recently.[35] TTL drives an increase in both tubulin mRNA and protein levels, perhaps through autoactivation.

Whereas *Vash1* mRNA level did not differ between the groups, *Vash2* mRNA level was very variable in KI-Empty mice and mRNA levels for both *Svbp* and *Tuba4a*, encoding a dTyr-tub isoform, were lower in KI-Empty (Figure 5J). TTL enhanced *Tuba4a* in KI mice (Figure 5F,J). The mRNA levels of tubulin polyglutamylases were dysregulated in KI-Empty, and TTL almost completely normalized *Ttll5* that prefers α- over β-tubulins in KI mice (Figure 5K). Several mRNAs encoding other microtubule-associated components were altered in KI-Empty and were not affected by TTL therapy, such as the molecular motors dyneins, dynactins and kinesins (Figure 5L-N), CAP-Gly domain-containing linker proteins (CLIPs), microtubule-associated proteins (MAPs) and microtubule-associated protein RP/EB family members (MAPREs; Figure 5O,P).

Proteome analysis revealed only a few dysregulated proteins that were normalized with TTL treatment. This is the case for KIF15, which was the only kinesin isoform detected by proteomics and its level was higher in KI-Empty and fully normalized by TTL treatment (Figure 5Q). Similarly, several mitochondrial proteins were normalized by TTL treatment, such as ornithine aminotransferase (OAT), pantothenate aminotransferase (PANK4), succinate-CoA ligase GDP/ADP-forming subunit alpha (SUCLG1), NFU1 iron-sulfur cluster scaffold (NFU1), hydroxysteroid 17-beta dehydrogenase 10 (HSD17B10) and electron transfer flavoprotein subunit beta (ETFB; Figure 5Q). Finally, three proteins that were more abundant in KI-Empty were even more accumulated in KI-TTL mice: CLIP1 (clip-170), which binds to the +end of microtubules and promotes their growth and bundling, IVD (isovaryl-CoA dehydrogenase), involved in leucine catabolism, and CAVIN4, which plays an important role in cardiomyocytes by interacting with stromal interaction molecule 1 (STIM1) to facilitate the store-operated calcium entry (SOCE) and the caveolae formation (Figure 5Q).[36]

Reduced tubulin detyrosination improved contractility in hiPSC-engineered heart tissues

To translate our mouse data to humans, hiPSC lines deficient in SVBP or TTL were created from a WT hiPSC line (mTag-RFP-T-TUBA1B) with CRISPR/Cas9 genetic tools (Figure S1A-D) and differentiated into cardiomyocytes. RT-qPCR confirmed the respective deficiency of SVBP and TTL mRNAs in hiPSC-cardiomyocytes (Figure S1E,F). SVBP-KO and TTL-KO hiPSC-derived cardiomyocytes respectively exhibited a markedly lower and higher dTyr-tub immunofluorescence intensity (Figure 6A) and protein levels (Figure 6B), confirming the targeting of either protein in hiPSC lines. Like the effect of TTL therapy in KI mice, tubulin detyrosination was not completely abolished in SVBP-KO, suggesting a role for TUBA4A and/or the recently discovered MATCAP1[37] in this process.

Then EHTs from the 3 genotypes were cast either on standard posts (0.28 mN/mm) or on stiffer posts that enhance afterload (0.8 mN/mm) and evaluated at the age of 60 days. On standard posts, force amplitude did not significantly differ between the groups, time to 50% peak (TTP_{50}) was longer in SVBP-KO and did not differ to WT in TTL-KO (Figure 6C). Conversely, time from peak to 50% relaxation (RT_{50}) was longer in TTL-KO and did not differ from the WT in SVBP-KO (Figure 6C). On stiffer posts, force amplitude and TTP_{50} were significantly higher, whereas RT_{50} was shorter in SVBP-KO (Figure 6D). In TTL-KO EHTs, force amplitude was lower, and kinetics were not significantly altered, but a trend towards longer RT_{50} was noticeable (Figure 6D). Therefore, stiffer posts were required to reveal an opposite phenotype in SVBP-KO and TTL-KO. These data provide evidence in a human cellular context that reducing tubulin detyrosination (=SVBP-KO) improved contractility in

human EHTs, whereas increasing tubulin detyrosination (=TTL-KO) leads to contractility impairment.

RNA-seq and mass spectrometry analyses were then performed in EHTs from WT on standard posts and on WT, SVBP-KO and TTL-KO on stiff posts. GO analysis of RNA-seq data revealed that stiffer posts induced an enrichment (log2 ratio >0.58, $p<0.05$) in components of mitochondria and of metabolic process, suggesting maturation in WT EHTs (Figure S5L, dataset 3). SVBP-KO exhibited enrichment vs. TTL-KO in components of extracellular matrix, endoplasmic reticulum, Golgi, plasma membrane, and sarcomere, associated with an enrichment in developmental process, response to stimulus, actin filament-based process, regulation of proteolysis and muscle contraction (Figure S5B, dataset 3). Conversely, TTL-KO showed enrichment vs. SVBP-KO in components of mitochondria, ribosome, RNA-binding, polysome, nucleus, associated with enrichment in process of oxidative phosphorylation, mitochondrial electron transport, translation, mRNA degradation, and several other metabolic process (Figure S5, dataset 3).

GO analysis of MS data showed enrichment in components of extracellular exosomes, vesicles and mitochondria in WT EHTs cast on stiffer posts (Figure S5D, dataset 4). SVBP-KO exhibited enrichment vs. TTL-KO in several cardiomyocyte components, including stress and contractile fibers, actin cytoskeleton, costamere, intracellular organelles, Z-disc and intercalated disc proteins, which were involved in cytoskeletal and actinin protein binding, actin filament-based process, muscle contraction, exocytosis and gluconeogenesis (Figure S5G, dataset 4). Conversely, GO analysis of TTL-KO showed enrichment vs. SVBP-KO in components of endoplasmic reticulum, Golgi, mitochondria, and secreted vesicles, which were involved in intracellular transport, metabolic process, negative regulation of proteolysis and response to stress (Figure S5H, dataset 4).

Discussion

This study evaluated the impact of targeting tubulin detyrosination by AAV9-mediated TTL gene transfer *in vivo* and in a human cellular model deficient in SVBP or TTL. The main findings are: i) TTL dose-dependently reduced tubulin detyrosination and improved cardiomyocyte contractility without affecting calcium transients in WT cardiomyocytes; ii) TTL partially improved LV function and diastolic filling, reduced stiffness without impact on TTN isoform composition and normalized cardiac output and stroke volume in KI mice; iii) TTL induced a marked transcription and translation of several tubulin isoforms in KI mice; iv) TTL modulated mRNA or protein levels of components of mitochondria, sarcomere Z-disc, ribosomal subunits, intercalated disc, lysosome and cytoskeleton in KI mice; v) SVBP-KO and TTL-KO EHTs exhibited low and high dTyr-tub levels, higher and lower force of contraction and enhanced and prolonged relaxation than in WT EHTs, respectively; vi) RNA-seq and mass spectrometry analysis revealed distinct enrichment of cardiomyocyte components and pathways in SVBP-KO and TTL-KO EHTs.

KI mice exhibited lower EF, SV, CO and dP/dt_{min} and higher LVM/BW, HW/BW and HW/TL, supporting reduced systolic and diastolic function and LV hypertrophy, as shown previously.[10, 11, 23] In addition, the expression of several genes involved in heart failure and autophagy-lysosomal pathway were dysregulated in KI mice, as reported previously.[34] In this study, we also show that the mRNA levels of several microtubule-associated proteins, such as dyneins, dynactins, kinesins, CLIPs, MAPs and MAPREs are higher in KI than in WT mice. This suggests a broad up-regulation of a microtubule-transport program in KI mice. Proteomic analysis revealed higher abundance of sarcomeric, cytoskeletal and intercalated disc proteins, such as MYH7, DES, TCAP, FHL1, PGM5, XIRP1, and MYOT, and of components of the proteasome core complex, such as PSMA6, PSMB5 and PSMD11, supporting previous findings of increased proteasomal activity at this age.[38] Interestingly the protein levels of the kinesin isoform KIF15, SLMAP and SORBS2 involved in myofibril assembly were also higher.

In the crude cardiac protein fraction, the level of dTyr-tub/GAPDH did not differ between KI- and WT-Empty as previously shown,[2] but the dTyr-tub/α-tubulin was slightly higher but did not reach significance in KI-Empty. TTL gene transfer dose-dependently reduced microtubule detyrosination in WT mice, supporting previous findings in human intact cardiomyocytes.[9] Microtubule detyrosination was also lower in *Mybpc3*-KI mice treated with TTL, but remained at about 60% of the WT. This could be explained by the marked accumulation of both TUBA4A mRNA and protein, which is the only tubulin isoform translated as detyrosinated,[4, 7] rather than a transcriptional upregulation of the VASH1/SVBP complex or the detyrosinase MATCAP1[37] (not shown) in KI-TTL mice.

Chronic TTL treatment reduced stiffness and improved fractional shortening and velocities of contraction and relaxation in a dose-dependent manner in cardiomyocytes isolated from WT rats. In HCM KI mice, chronic TTL treatment ameliorated EF, SV and CO, markedly increased diastolic filling and reduced stiffness. The latter was not associated with a shift of compliant-to-stiff TTN isoform in KI mice. On the other hand, TTL did not improve diastolic function (dP/dt_{min}) and had no impact on LV hypertrophy, except for an amelioration of the VW/BW and VW/TL ratios in female KI-TTL mice. The positive impact of TTL overexpression on cardiac function in mice was supported by the findings of markedly reduced level of dTyr-tub/α-tubulin, higher force of contraction and faster relaxation in SVBP-KO hiPSC-derived cardiomyocytes and EHTs. Conversely, the TTL-KO cardiomyocytes and EHTs showed the opposite with >2-fold higher levels of dTyr-tub/α-tubulin, lower force of contraction and prolonged relaxation. These data provide evidence in a human cellular context that reducing tubulin detyrosination (=SVBP-KO) improved contractility in human EHTs, whereas increasing tubulin detyrosination (=TTL-KO) is associated with contractility impairment, mimicking the situation in several types of heart failure[2, 3] (for reviews,[4-7]).

Contractility findings in EHTs were supported by the RNA-seq and proteomic analyses, showing enrichment in components involved in muscle structure development, response to stimulus, cytoskeleton binding and function, and muscle contraction, whereas TTL-KO was rather enriched in components involved in oxidative phosphorylation, mitochondrial electron transport, translation, mRNA degradation, response to stress and other metabolic processes. Although RNA-seq and mass spectrometry data did not reveal the most likely candidates that could reduce stiffness in KI-TTL mice, GO pathway analysis revealed modulation of components of the cytoskeleton, mitochondria, metabolism, lysosome, sarcomere Z-disc and intercalated disc. At least the markedly higher level of CLIP1 in KI-TTL supports previous findings that CLIP1 binds to the +end of Tyr-tub and improves dynein-dynactin-mediated retrograde cargo transport.[39, 40] Similarly interesting was the higher protein level of MURC/CAVIN4 in KI-TTL, which interacts with STIM1 to facilitate the SOCE and the caveolae formation.[36] Finally, the markedly high protein level of kinesin KIF15 in KI mice was fully normalized with TTL. Although its role is not deciphered in the heart, it has shown to play a role in tubulin polymerization in other contexts.[41] Another interesting finding in our study is that most of tubulin isoforms exhibited lower mRNA and higher protein level in KI mice, such as observed in human heart failure samples.[35] In both models, TUBA1A, TUBB4B, TUBB2B and TUBB5 are more abundant, while TUBA1C, TUBB3 and TUBB6 proteins were not detected in our proteomic analysis. These data suggest that tubulin autoregulation, characterized by mRNA repression by abundant protein levels is effective in KI mice with hypertrophy and dysfunction, in agreement with previous work in human failing cardiomyocytes.[35] Interestingly, however, TTL did not reverse this phenotype, but stimulated transcription of most tubulin isoforms, leading to accumulation of both tubulin mRNAs and proteins. This suggests that TTL-bound tubulin protein is not able to trigger autoinhibition as it should, leading to tubulin mRNA autoactivation.

In conclusion, this study provides evidence that reducing dTyr-tub ameliorates contractility in both HCM mice and human EHTs and holds promise for further targeting the non-sarcomeric cytoskeleton in heart disease.

Acknowledgments

The authors gratefully acknowledge Moritz Meyer-Jens (Pharmacology, UKE, Hamburg) for contributing to the maintenance of hiPSCs, hiPSC-EHTs, the FACS core facility (UKE, Hamburg). We thank Zubayda Sultan and Jennifer Sarikaya (Amsterdam UMC) for the help in titin isoform analysis. We also would like to thank Thomas Eschenhagen and Marc Hirt (Pharmacology, UKE, Hamburg) for providing us with the standard and stiff silicone EHT posts. Finally, we thank Marie-Jo Moutin (GIN, Grenoble) for providing us with antibodies directed against tubulin modifications.

Source of Fundings

This worked was supported fully or in part by the Leducq Foundation (20CVD01) to LC, BP and JVDV, the German Centre for Cardiovascular Research (DZHK) and the German Ministry of Research Education (BMBF) to LC, and by the National Institute of Health (NIH) R01s-HL133080 and HL149891 to BP.

Disclosures

GM is now an employee at DiNAQOR AG. LC is a member of DiNAQOR Scientific Advisory Board and has shares in DiNAQOR. BLP is an inventor on a pending US Patent Application no. 15/959,181 for “Composition and Methods for Improving Heart Function and Treating Heart Failure”. The remaining authors declare no competing interests.

Data Availability Statement

Datasets, analysis and study materials will be made available on request to other researchers for the purpose of reproducing the results or replicating the procedures. All data of OMIC experiments have been or will be made publicly available. The RNA-seq data have been deposited to RNA-seq datasets to NCBI's Gene Expression Omnibus (GEO) of the European Nucleotide Archive (ENA) at EMBL-EBI, accession number is pending. The mass spectrometry proteomics data have been deposited to the ProteomeXchange Consortium via the PRIDE42 partner repository with the dataset identifier PXD042418.

References

1. Carrier L. Targeting the population for gene therapy with MYBPC3. *J Mol Cell Cardiol*. 2020;150:101-108. doi: 10.1016/j.yjmcc.2020.10.003
2. Schuldt M, Pei J, Harakalova M, Dorsch LM, Schlossarek S, Mokry M, Knol JC, Pham TV, Schelfhorst T, Piersma SR, Dos Remedios C, Dalinghaus M, Michels M, Asselbergs FW, Moutin MJ, Carrier L, Jimenez CR, van der Velden J, Kuster DWD. Proteomic and functional studies reveal detyrosinated tubulin as treatment target in sarcomere mutation-induced hypertrophic cardiomyopathy. *Circ Heart Fail*. 2021;14:e007022. doi: 10.1161/CIRCHEARTFAILURE.120.007022
3. Robison P, Caporizzo MA, Ahmadzadeh H, Bogush AI, Chen CY, Margulies KB, Shenoy VB, Prosser BL. Detyrosinated microtubules buckle and bear load in contracting cardiomyocytes. *Science*. 2016;352:aaf0659. doi: 10.1126/science.aaf0659
4. Sanyal C, Pietsch N, Ramirez Rios S, Peris L, Carrier L, Moutin MJ. The detyrosination/re-tyrosination cycle of tubulin and its role and dysfunction in neurons

and cardiomyocytes. *Semin Cell Dev Biol*. 2023;137:46-62. doi: 10.1016/j.semcdb.2021.12.006

5. Caporizzo MA, Chen CY, Prosser BL. Cardiac microtubules in health and heart disease. *Exp Biol Med (Maywood)*. 2019;244:1255-1272. doi: 10.1177/1535370219868960
6. Caporizzo MA, Prosser BL. The microtubule cytoskeleton in cardiac mechanics and heart failure. *Nat Rev Cardiol*. 2022;19:364-378. doi: 10.1038/s41569-022-00692-y
7. Uchida K, Scarborough EA, Prosser BL. Cardiomyocyte microtubules: Control of mechanics, transport, and remodeling. *Annu Rev Physiol*. 2022;84:257-283. doi: 10.1146/annurev-physiol-062421-040656
8. Chen CY, Caporizzo MA, Bedi K, Vite A, Bogush AI, Robison P, Heffler JG, Salomon AK, Kelly NA, Babu A, Morley MP, Margulies KB, Prosser BL. Suppression of detyrosinated microtubules improves cardiomyocyte function in human heart failure. *Nat Med*. 2018;24:1225-1233. doi: 10.1038/s41591-018-0046-2
9. Chen CY, Salomon AK, Caporizzo MA, Curry S, Kelly NA, Bedi K, Bogush AI, Kramer E, Schlossarek S, Janiak P, Moutin MJ, Carrier L, Margulies KB, Prosser BL. Depletion of vasohibin 1 speeds contraction and relaxation in failing human cardiomyocytes. *Circ Res*. 2020;127:e14-e27. doi: 10.1161/CIRCRESAHA.119.315947
10. Vignier N, Schlossarek S, Fraysse B, Mearini G, Kramer E, Pointu H, Mougenot N, Guiard J, Reimer R, Hohenberg H, Schwartz K, Vernet M, Eschenhagen T, Carrier L. Nonsense-mediated mrna decay and ubiquitin-proteasome system regulate cardiac myosin-binding protein c mutant levels in cardiomyopathic mice. *Circ Res*. 2009;105:239-248. doi: 10.1161/CIRCRESAHA.109.201251
11. Fraysse B, Weinberger F, Bardswell SC, Cuello F, Vignier N, Geertz B, Starbatty J, Kramer E, Coirault C, Eschenhagen T, Kentish JC, Avkiran M, Carrier L. Increased myofilament Ca(2+) sensitivity and diastolic dysfunction as early consequences of *Mybpc3* mutation in heterozygous knock-in mice. *J Mol Cell Cardiol*. 2012;52:1299-1307. doi: 10.1016/j.yjmcc.2012.03.009
12. Kerr JP, Robison P, Shi G, Bogush AI, Kempema AM, Hexum JK, Becerra N, Harki DA, Martin SS, Raiteri R, Prosser BL, Ward CW. Detyrosinated microtubules modulate mechanotransduction in heart and skeletal muscle. *Nat Commun*. 2015;6:8526. doi: 10.1038/ncomms9526
13. Caporizzo MA, Chen CY, Salomon AK, Margulies KB, Prosser BL. Microtubules provide a viscoelastic resistance to myocyte motion. *Biophys J*. 2018;115:1796-1807. doi: 10.1016/j.bpj.2018.09.019
14. Concordet JP, Haeussler M. Crispor: Intuitive guide selection for crispr/cas9 genome editing experiments and screens. *Nucleic Acids Res*. 2018;46:W242-W245. doi: 10.1093/nar/gky354
15. Mosqueira D, Mannhardt I, Bhagwan JR, Lis-Slimak K, Katili P, Scott E, Hassan M, Prondzynski M, Harmer SC, Tinker A, Smith JGW, Carrier L, Williams PM, Gaffney D, Eschenhagen T, Hansen A, Denning C. Crispr/cas9 editing in human pluripotent stem cell-cardiomyocytes highlights arrhythmias, hypocontractility, and energy depletion as potential therapeutic targets for hypertrophic cardiomyopathy. *Eur Heart J*. 2018;39:3879-3892. doi: 10.1093/eurheartj/ehy249
16. Prondzynski M, Lemoine MD, Zech AT, Horvath A, Di Mauro V, Koivumaki JT, Kresin N, Busch J, Krause T, Kramer E, Schlossarek S, Spohn M, Friedrich FW, Munch J, Laufer SD, Redwood C, Volk AE, Hansen A, Mearini G, Catalucci D, Meyer C, Christ T, Patten M, Eschenhagen T, Carrier L. Disease modeling of a mutation in alpha-actinin 2 guides clinical therapy in hypertrophic cardiomyopathy. *EMBO Mol Med*. 2019;11:e11115. doi: 10.15252/emmm.201911115
17. Rhoden A, Schulze T, Pietsch N, Christ T, Hansen A, Eschenhagen T. Comprehensive analyses of the inotropic compound omecamtiv mecarbil in rat and human cardiac preparations. *Am J Physiol Heart Circ Physiol*. 2022;322:H373-H385. doi: 10.1152/ajpheart.00534.2021

18. Zech ATL, Prondzynski M, Singh SR, Pietsch N, Orthey E, Alizoti E, Busch J, Madsen A, Behrens CS, Meyer-Jens M, Mearini G, Lemoine MD, Kramer E, Mosqueira D, Virdi S, Indenbirken D, Depke M, Salazar MG, Volker U, Braren I, Pu WT, Eschenhagen T, Hammer E, Schlossarek S, Carrier L. *ACTN2* mutant causes proteopathy in human ipsc-derived cardiomyocytes. *Cells*. 2022;11doi: 10.3390/cells11172745
19. Lock M, McGorray S, Auricchio A, Ayuso E, Beecham EJ, Blouin-Tavel V, Bosch F, Bose M, Byrne BJ, Caton T, Chiorini JA, Chtarto A, Clark KR, Conlon T, Darmon C, Doria M, Douar A, Flotte TR, Francis JD, Francois A, Giacca M, Korn MT, Korytov I, Leon X, Leuchs B, Lux G, Melas C, Mizukami H, Moullier P, Muller M, Ozawa K, Philipsberg T, Poulard K, Raupp C, Riviere C, Roosendaal SD, Samulski RJ, Soltys SM, Surosky R, Tenenbaum L, Thomas DL, van Montfort B, Veres G, Wright JF, Xu Y, Zelenaia O, Zentilin L, Snyder RO. Characterization of a recombinant adeno-associated virus type 2 reference standard material. *Hum Gene Ther*. 2010;21:1273-1285. doi: 10.1089/hum.2009.223
20. Lock M, Alvira MR, Chen SJ, Wilson JM. Absolute determination of single-stranded and self-complementary adeno-associated viral vector genome titers by droplet digital pcr. *Hum Gene Ther Methods*. 2014;25:115-125. doi: 10.1089/hgtb.2013.131
21. Mearini G, Stimpel D, Kramer E, Geertz B, Braren I, Gedicke-Hornung C, Precigout G, Muller OJ, Katus HA, Eschenhagen T, Voit T, Garcia L, Lorain S, Carrier L. Repair of *Mybpc3* mRNA by 5'-trans-splicing in a mouse model of hypertrophic cardiomyopathy. *Mol Ther Nucleic Acids*. 2013;2:e102. doi: 10.1038/mtna.2013.31
22. Gedicke-Hornung C, Behrens-Gawlik V, Reischmann S, Geertz B, Stimpel D, Weinberger F, Schlossarek S, Precigout G, Braren I, Eschenhagen T, Mearini G, Lorain S, Voit T, Dreyfus PA, Garcia L, Carrier L. Rescue of cardiomyopathy through u7snrna-mediated exon skipping in *Mybpc3*-targeted knock-in mice. *EMBO Mol Med*. 2013;5:1128-1145. doi: 10.1002/emmm.201202168
23. Mearini G, Stimpel D, Geertz B, Weinberger F, Krämer E, Schlossarek S, Mourot-Filiatre J, Stöhr A, Dutshc A, Wijnker PJM, Braren I, Katus HA, Müller OJ, Voit T, Eschenhagen T, Carrier L. *Mybpc3* gene therapy for neonatal cardiomyopathy enables longterm disease prevention in mice. *Nat Commun*. 2014;5:5515. doi: 10.1038/ncomms6515
24. Pacher P, Nagayama T, Mukhopadhyay P, Batkai S, Kass DA. Measurement of cardiac function using pressure-volume conductance catheter technique in mice and rats. *Nat Protoc*. 2008;3:1422-1434. doi: 10.1038/nprot.2008.138
25. Hinrichs S, Scherschel K, Kruger S, Neumann JT, Schwarzl M, Yan I, Warnke S, Ojeda FM, Zeller T, Karakas M, Keller T, Meyer C, Blankenberg S, Westermann D, Lindner D. Precursor proadrenomedullin influences cardiomyocyte survival and local inflammation related to myocardial infarction. *Proc Natl Acad Sci U S A*. 2018;115:E8727-E8736. doi: 10.1073/pnas.1721635115
26. Bacmeister L, Segin S, Medert R, Lindner D, Freichel M, Camacho Londono JE. Assessment of peep-ventilation and the time point of parallel-conductance determination for pressure-volume analysis under beta-adrenergic stimulation in mice. *Front Cardiovasc Med*. 2019;6:36. doi: 10.3389/fcvm.2019.00036
27. Warren CM, Jordan MC, Roos KP, Krzesinski PR, Greaser ML. Titin isoform expression in normal and hypertensive myocardium. *Cardiovasc Res*. 2003;59:86-94. doi: 10.1016/s0008-6363(03)00328-6
28. Bolger AM, Lohse M, Usadel B. Trimmomatic: A flexible trimmer for illumina sequence data. *Bioinformatics*. 2014;30:2114-2120. doi: 10.1093/bioinformatics/btu170
29. Kim D, Paggi JM, Park C, Bennett C, Salzberg SL. Graph-based genome alignment and genotyping with hisat2 and hisat-genotype. *Nat Biotechnol*. 2019;37:907-915. doi: 10.1038/s41587-019-0201-4
30. Li H, Handsaker B, Wysoker A, Fennell T, Ruan J, Homer N, Marth G, Abecasis G, Durbin R, Genome Project Data Processing S. The sequence alignment/map format and samtools. *Bioinformatics*. 2009;25:2078-2079. doi: 10.1093/bioinformatics/btp352

31. Anders S, Pyl PT, Huber W. Htseq--a python framework to work with high-throughput sequencing data. *Bioinformatics*. 2015;31:166-169. doi: 10.1093/bioinformatics/btu638
32. Love MI, Huber W, Anders S. Moderated estimation of fold change and dispersion for rna-seq data with deseq2. *Genome Biol*. 2014;15:550. doi: 10.1186/s13059-014-0550-8
33. Raudvere U, Kolberg L, Kuzmin I, Arak T, Adler P, Peterson H, Vilo J. G:Profiler: A web server for functional enrichment analysis and conversions of gene lists (2019 update). *Nucleic Acids Res*. 2019;47:W191-W198. doi: 10.1093/nar/gkz369
34. Singh SR, Zech ATL, Geertz B, Reischmann-Dusener S, Osinska H, Prondzynski M, Kramer E, Meng Q, Redwood C, van der Velden J, Robbins J, Schlossarek S, Carrier L. Activation of autophagy ameliorates cardiomyopathy in *Mybpc3*-targeted knockin mice. *Circ Heart Fail*. 2017;10doi: 10.1161/CIRCHEARTFAILURE.117.004140
35. Phyo SA, Uchida K, Chen CY, Caporizzo MA, Bedi K, Griffin J, Margulies K, Prosser BL. Transcriptional, post-transcriptional, and post-translational mechanisms rewrite the tubulin code during cardiac hypertrophy and failure. *Front Cell Dev Biol*. 2022;10:837486. doi: 10.3389/fcell.2022.837486
36. Malette J, Degrandmaison J, Giguere H, Berthiaume J, Frappier M, Parent JL, Auger-Messier M, Boulay G. Murc/cavin-4 facilitates store-operated calcium entry in neonatal cardiomyocytes. *Biochim Biophys Acta Mol Cell Res*. 2019;1866:1249-1259. doi: 10.1016/j.bbamcr.2019.03.017
37. Landskron L, Bak J, Adamopoulos A, Kaplani K, Moraiti M, van den Hengel LG, Song JY, Bleijerveld OB, Nieuwenhuis J, Heidebrecht T, Henneman L, Moutin MJ, Barisic M, Taraviras S, Perrakis A, Brummelkamp TR. Posttranslational modification of microtubules by the MATCAP detyrosinase. *Science*. 2022;376:eabn6020. doi: 10.1126/science.abn6020
38. Schlossarek S, Englmann DR, Sultan KR, Sauer M, Eschenhagen T, Carrier L. Defective proteolytic systems in mybpc3-targeted mice with cardiac hypertrophy. *Basic Res Cardiol*. 2012;107:1-13. doi: 10.1007/s00395-011-0235-3
39. Peris L, Thery M, Faure J, Saoudi Y, Lafanechere L, Chilton JK, Gordon-Weeks P, Galjart N, Bornens M, Wordeman L, Wehland J, Andrieux A, Job D. Tubulin tyrosination is a major factor affecting the recruitment of cap-gly proteins at microtubule plus ends. *J Cell Biol*. 2006;174:839-849. doi: 10.1083/jcb.200512058
40. Nirschl JJ, Magiera MM, Lazarus JE, Janke C, Holzbaur EL. Alpha-tubulin tyrosination and clip-170 phosphorylation regulate the initiation of dynein-driven transport in neurons. *Cell Rep*. 2016;14:2637-2652. doi: 10.1016/j.celrep.2016.02.046
41. Wu S, Lv L, Li L, Wang L, Mao B, Li J, Shen X, Ge R, Wong CKC, Sun F, Cheng CY. Kif15 supports spermatogenesis via its effects on sertoli cell microtubule, actin, vimentin, and septin cytoskeletons. *Endocrinology*. 2021;162doi: 10.1210/endocr/bqab010
42. Perez-Riverol Y, Bai J, Bandla C, Garcia-Seisdedos D, Hewapathirana S, Kamatchinathan S, Kundu DJ, Prakash A, Frericks-Zipper A, Eisenacher M, Walzer M, Wang S, Brazma A, Vizcaino JA. The pride database resources in 2022: A hub for mass spectrometry-based proteomics evidences. *Nucleic Acids Res*. 2022;50:D543-D552. doi: 10.1093/nar/gkab1038

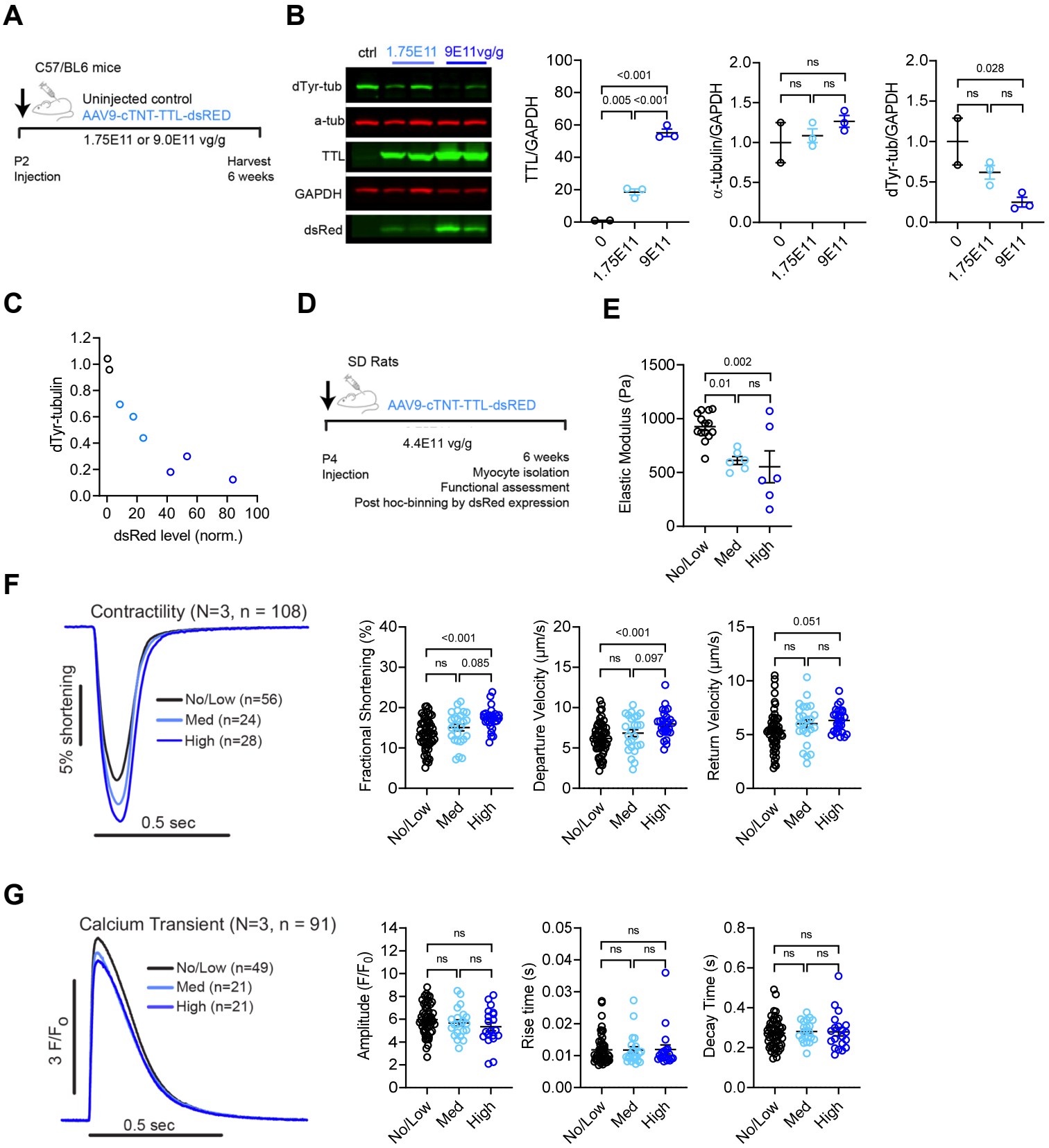

Figure 1. Effect of *TTL* gene transfer in wild-type rodents and analysis on isolated cardiomyocytes. A) Protocol. Wild-type neonatal mice (P2) received either an adeno-associated virus serotype (AAV9) encoding TTL-dsRed at a low (1.75E11 vg/g, N=3) or high dose (9E11 vg/g, N=3), or a sham injection (N=2). After 6 weeks, ventricular myocardium was harvested. **B)** Representative Western blot and quantification of TTL, total α-tubulin and detyrosinated tubulin (dTyr-tub), normalized to GAPDH. **C)** Correlation between dsRed protein level (measured via Western blot) and dTyr-tub levels from the same hearts in B. **D)** Protocol. Wild-type neonatal Sprague Dawley rats (P4) received an AAV9 encoding TTL-dsRed at an intermediate dose (4.4E11 vg/g, N=3). After 6 weeks, single ventricular myocytes were isolated and functionally assessed. Following assessment, myocytes were binned into tertiles based on no/low, medium, or high level of TTL (indicated by dsRed fluorescence intensity). **E)** Myocyte stiffness (elastic modulus) measured via transverse nanoindentation. **F)** Sarcomere shortening representative traces and quantification of fractional shortening, contraction and relaxation velocity. **G)** Calcium transient representative traces and quantification of amplitude, rise time and decay time. Data are expressed as mean ± SEM with N/n representing the number of analysed mice and cardiomyocytes, respectively. Statistical significance assessed via one-way ANOVA with post hoc Tukey test for multiple comparisons. Abbreviation: ns, P>0.1

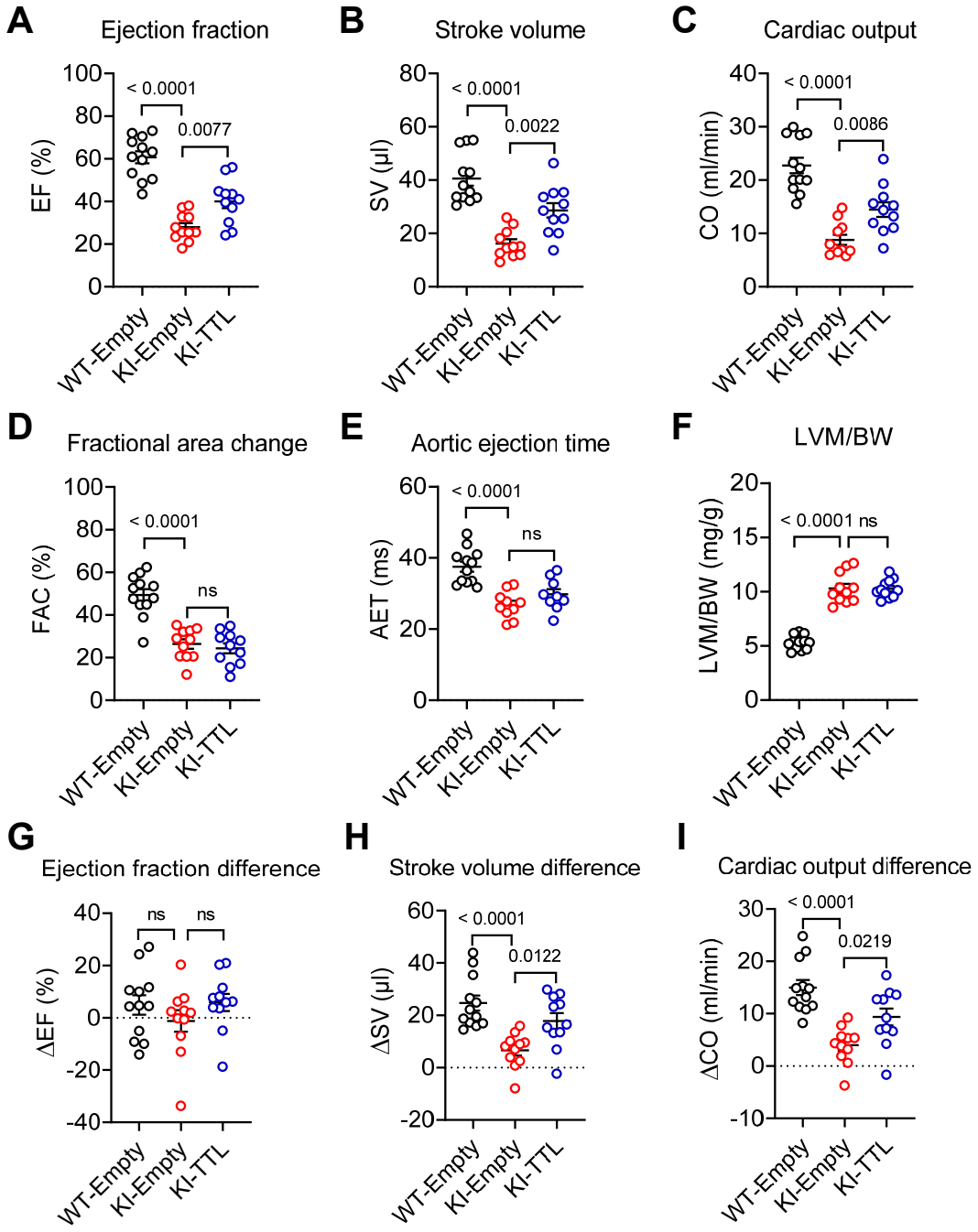

Figure 2. Evaluation of the cardiac phenotype by echocardiography after a 12-week AAV9-TTL/-Empty treatment. Three-week-old wild-type (WT) and *Mybpc3*-targeted knock-in (KI) mice were included in the study. Mice received either AAV9-Empty (no insert) or AAV9-TTL (HA-tagged human TTL). **A)** Ejection fraction (EF), **B)** Stroke volume (SV), **C)** Cardiac output (CO), **D)** Fractional area change (FAC), **E)** Aortic ejection time (AOT), **F)** Left ventricular mass to body weight ratio (LVM/BW). Difference in parameter values obtained between last and first echocardiography for **G)** Ejection fraction (DEF), **H)** Stroke volume (DSV) and **I)** Cardiac output (DCO). Data are expressed as mean ± SEM; **P<0.01 and ****P<0.0001 vs. KI-Empty, one-way ANOVA, followed by Dunnett's post-test. Abbreviation: ns, P>0.1.

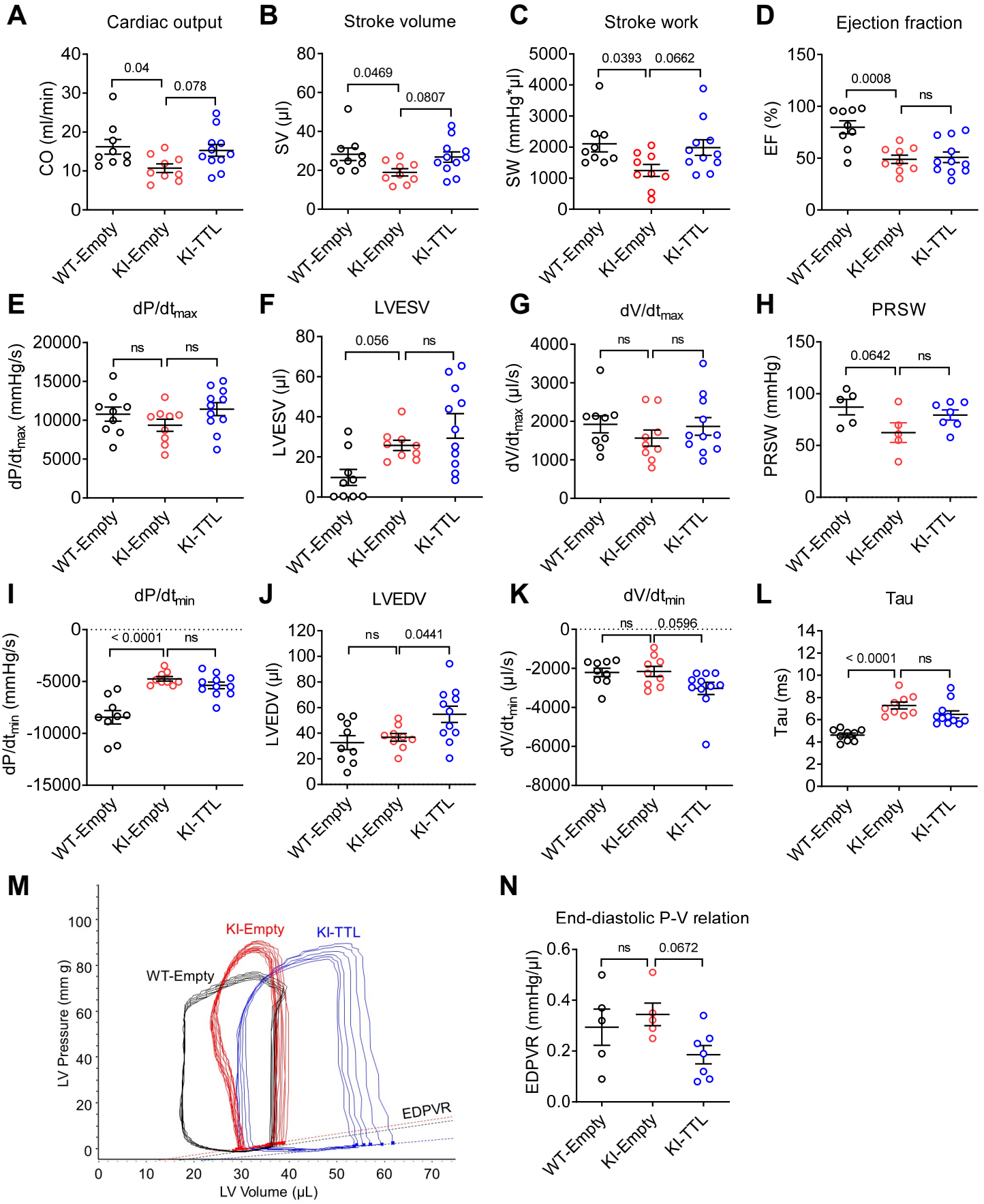

Figure 3. Evaluation of the cardiac phenotype by hemodynamics after a 12-week AAV9-TTL/-Empty treatment. Three-week-old wild-type (WT) and *Mybpc3*-targeted knock-in (KI) mice were included in the study (N=9-11). Mice received either AAV9-Empty (no insert) or AAV9-TTL (HA-tagged human TTL). **A)** Cardiac output (CO), **B)** Stroke volume (SV), **C)** Stroke work (SW), **D)** Ejection fraction (EF), **E)** Maximum rate of left ventricular pressure change (dP/dt_{max}), **F)** Left ventricular end-systolic volume (Ves), **G)** Maximal rate of left ventricular volume change (dV/dt_{max}), **H)** Preload recruitable stroke work (PRSW), **I)** Minimal rate of left ventricular pressure change (dP/dt_{min}), **J)** LV End-diastolic volume (Ved), **K)** Minimal rate of left ventricular volume change (dV/dt_{min}), **L)** Time constant of active relaxation (Tau), calculated with the Weiss method, **M)** PV-loop traced after increasing occlusion in a representative mouse of each performed group, **N)** End-diastolic pressure-volume relation (EDPVR), calculated with a linear fit. Data are expressed as mean ± SEM. P values vs. KI-Empty were obtained with one-way ANOVA, followed by Dunnett's multiple comparisons test. Abbreviation: N, number of mice; ns, P>0.1.

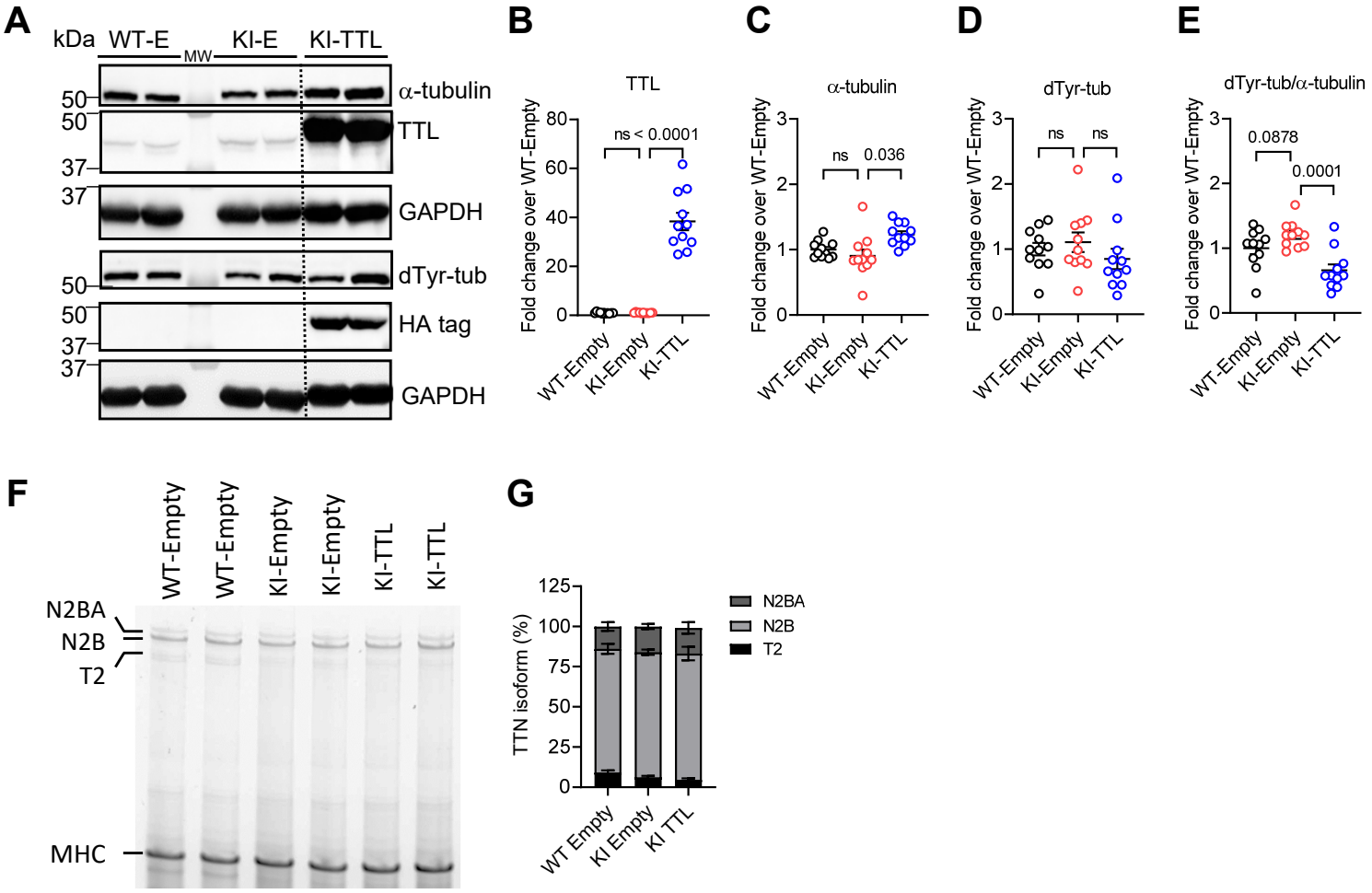

Figure 4. Molecular evaluation of tubulin modifications and titin isoforms in mice. A) Representative Western blot of cardiac crude protein fractions stained for α-tubulin, tubulin tyrosine ligase (TTL), detyrosinated tubulin (dTyr-tub), HA tag, and for GAPDH as a loading control in WT-Empty (WT-E), KI-Empty (KI-E) and KI-TTL mice (N=11); dashed line indicates where the blots were cut. **B)** TTL, **C)** α-tubulin, **D)** dTyr-tub and **E)** dTyr-tub/α-tubulin protein levels. **F)** Representative Western blot of cardiac crude protein fractions stained for titin (isoforms N2BA, N2B and T2) and myosin heavy chain (MHC). **G)** Percentage of N2BA, N2B and T2 isoforms normalized to MHC (N=5, 8, 8 in WT-Empty, KI-Empty and KI-TTL). Data in panels B-E and G-L are expressed as mean ± SEM and relative to the mean of WT-Empty. P values vs. KI-Empty were obtained with one-way ANOVA, followed by Dunnett's multiple comparisons test. Abbreviation: N, number of mice; ns, P>0.1.

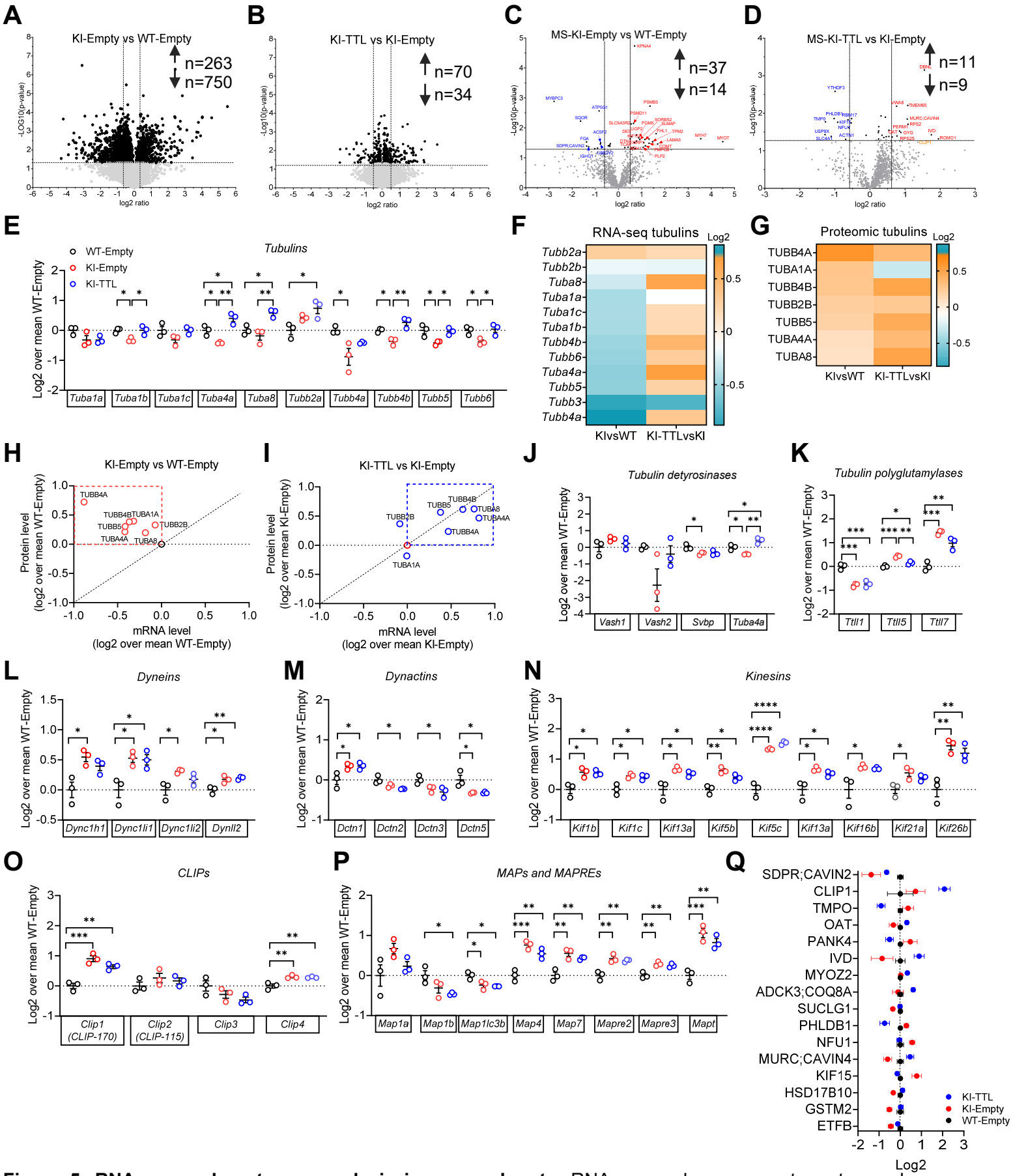

Figure 5. RNA-seq and proteome analysis in mouse hearts. RNA-seq and mass spectrometry analysis were performed in female mouse LV tissue extracts (N=3). Volcano plots show the -Log10 of P-value vs. the magnitude of change (log2 ratio) of **A)** mRNA levels in KI-Empty/WT-Empty, **B)** mRNA levels in KI-TTL/KI-Empty, **C)** protein levels in KI-Empty/ WT-Empty and **D)** protein levels in KI-TTL/KI-Empty; light grey dots indicate P>0.05 and dark grey dots P<0.05. **E)** tubulin mRNA levels over WT-Empty. **F)** tubulin mRNA levels in KI-Empty/WT-Empty (left) and in KI-TTL/KI-Empty (right). **G)** tubulin protein levels in KI-Empty/WT-Empty (left) and in KI-TTL/KI-Empty (right). Correlation of log2 ratio of tubulin mRNA and protein levels in **H)** KI-Empty/WT-Empty and **I)** KI-TTL/KI-Empty. **(J-P)** mRNA levels over WT-Empty of **J)** tubulin detyrosinases, **K)** tubulin polyglutamylases, **L)** dyneins, **M)** dynactins, **N)** kinesins, **O)** CAP-GLY domain containing linker proteins (CLIPs), **P)** microtubule-associated proteins (MAPs) and protein RP/EB family members (MAPREs). **Q)** significantly dysregulated proteins over mean WT-Empty. Data are expressed as log2 mean ± SEM over mean of WT-Empty or KI-Empty; *P<0.01, **P<0.01 and ****P<0.0001 vs. KI-Empty, one-way ANOVA, followed by Tukey's post-test.

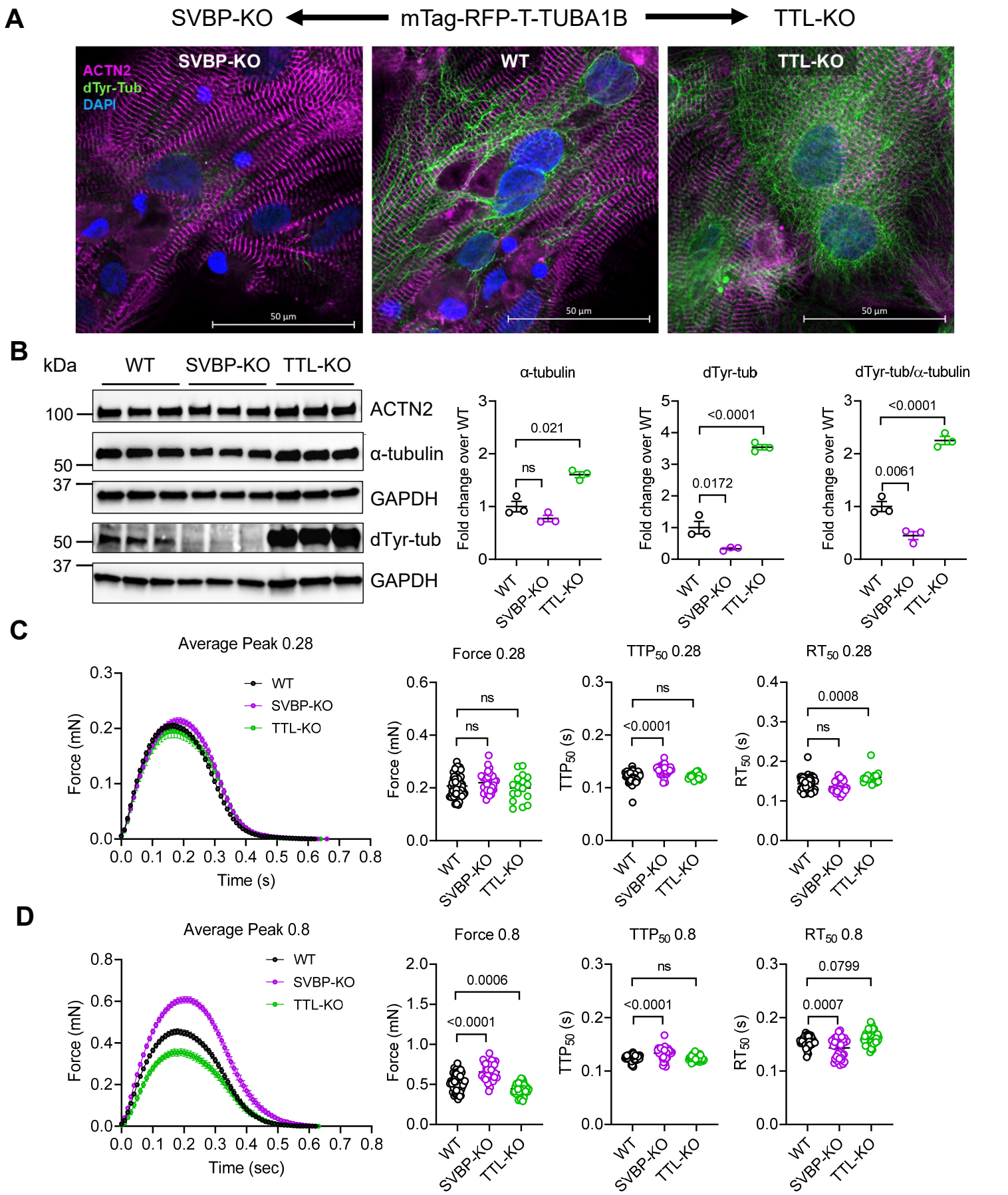

Figure 6. Evaluation of SVBP-KO and TTL-KO hiPSC-derived cardiomyocytes and engineered heart tissues. SVBP-KO and TTL-KO hiPSC lines were created from a control wild-type hiPSC line (WT, mTag-RFP-T-TUBA1B) with CRISPR/Cas9 genetic tools and differentiated into cardiomyocytes and engineered heart tissues (EHTs). **A)** Immunofluorescence analysis of 30-day-old SVBP-KO, WT and TTL-KO hiPSC-cardiomyocytes stained for α-actinin 2 (ACTN2, purple), detyrosinated α-tubulin (dTyr-tub, green) and DAPI (blue). Bar scale = 50 µm. **B)** Western blot and performed on 30-day-old hiPSC-cardiomyocytes (N=3) stained for ACTN2, α-tubulin, dTyr-tub and for GAPDH, as a loading control. Quantification of α-tubulin, dTyr-tub and dTyr-tub/α-tubulin protein levels relative to WT mean. HiPSC-derived cardiomyocytes were cast in EHTs and cultivated for 60 days. Measurements of average peak, force amplitude, time to 50% of peak (TTP_{50}) and time to 50% relaxation (RT_{50}) of 60-day-old EHTs cast on **C)** standard posts (0.28 mN/mm; WT: N/d = 75/6, SVBP-KO: N/d = 33/5, TTL-KO: N/d = 17/2) or **D)** afterload enhanced posts (0.8 mN/mm; WT: N/d = 54/6, SVBP-KO: N/d = 33/5, TTL-KO: N/d = 38/5). Data are expressed as mean ± SEM, with P values vs. WT obtained with a one-way ANOVA, followed by a Dunnett's post-test. Abbreviations: N/d, number of EHTs/differentiations; ns, P>0.1